RSC Advances

PAPER

Cite this: *RSC Adv.*, 2021, **11**, 3751

Nanochannel-based sensor for the detection of lead ions in traditional Chinese medicine†

Jiyuan Tu,[ab] Zhongshi Zhou,[a] Yanju Liu,[ab] Tingxian Li,[a] Shumin Lu,[c] Ling Xiao,[a] Pingping Xiao,[c] Guojun Zhang*[c] and Zhongyue Sun *[c]

Lead ions (Pb^{2+}) are used in the quality control of traditional Chinese medicine (TCM) preparations because they are highly toxic to human health. At present, sophisticated analytical instrumentation and complicated procedures for sample analysis are needed for the determination of Pb^{2+}. Herein, a simple, fast, and sensitive peptide-modified nanochannel sensor to detect Pb^{2+} in TCM is reported, which is based on a Pb^{2+}-specific peptide modified porous anodized aluminum membrane (PAAM). This peptide-based nanochannel clearly has the highest selectivity for Pb^{2+} when compared to other heavy metal ions, including As^{2+}, Cd^{3+}, Co^{2+}, Cr^{2+}, Cu^{2+}, Fe^{3+}, Hg^{2+}, Mg^{2+}, Mn^{2+}, Ni^{2+}, and Zn^{2+}. Based on linear ranges from 0.01 to 0.16 μM and 10 to 100 μM, the detection limit was calculated to be 0.005 μM. Moreover, this peptide-based nanochannel sensor was successfully used to detect Pb^{2+} in complex TCM samples. In addition, when compared with the gold standard atomic absorption spectrophotometry (AAS) method, the recovery of the peptide-modified nanochannel sensor was between 87.7% and 116.8%. The experimental results prove that this new sensor is able to achieve accurate detection of Pb^{2+} in TCM samples. Thus, this sensor system could provide a simple assay for sensitive and selective detection of Pb^{2+} in TCM, thereby showing great potential in the practical application for the quality control of heavy metals in TCM.

Received 2nd December 2020
Accepted 31st December 2020

DOI: 10.1039/d0ra10157e

rsc.li/rsc-advances

Introduction

Traditional Chinese medicine (TCM) has a long history over thousands of years due to its synergistic, effect-enhanced, clinical efficacy.[1–4] Yet, TCM differs from modern medicine, which contains a single active constituent and supplementary material with a quantitative concentration. The TCM has multiple active constituents and other compounds including toxic components, and their concentrations are influenced by origin and processing techniques.[5] These characteristics prove to be a great challenge when determining the quality and safety profile of TCM. Nowadays, the safety issues associated with TCM are of significant public concern.[6] The heavy metal pollution of TCM is currently a serious safety concern and has become the key to TCM quality control.[7] Previous studies have reported on heavy metal toxicity in TCM.[8,9] Based on these studies, the limitation of TCM heavy metals has played an important role in the pharmacopoeia of various countries, including the *Chinese Pharmacopoeia*, 2020 edition.[10] Among all the toxic metals, lead (Pb^{2+}) has received considerable attention as a representative of the heavy metal pollutants and is a serious hazard because of its ability to damage the central nervous system,[11,12] the kidneys,[12] the cardiovascular system,[13] the reproductive organs[14] and the hematological system.[15] Pb^{2+} ions are one of the key elements in the quality control of TCM. Thus, new analytical techniques that are capable of rapidly and sensitively detecting lead in TCM samples are of utmost importance.

For detecting Pb^{2+} in TCM, analytical tools, such as atomic absorption spectrometry (AAS), fluorescence spectroscopy (FL), inductively coupled plasma mass spectrometry (ICP-MS), and spectrophotometry have been applied.[16] These methods, however, lack the ability to be used for real-time and on-site monitoring. Although these techniques are accurate and highly sensitive for detection, better methodological features for ease of operation and low cost need to be investigated. The latest findings revealed that an electrochemical method can play an important role in the detection of toxic metal ions because of its high sensitivity, simple instrumentation, low production cost, fast response, and portability. Dahaghin *et al.*[17] developed a novel ion imprinted polymer electrochemical sensor for the selective detection of Pb^{2+}. Moreover, Shah *et al.*[18] developed a highly sensitive electrochemical sensing platform for trace level detection of Pb^{2+}.

[a]*School of Pharmacy, Hubei University of Chinese Medicine, 1 Huangjia Lake West Road, Wuhan 430065, PR China*

[b]*Hubei Research Center of Chinese Materia Medica Processing Engineering and Technology, Hubei University of Chinese Medicine, 1 Huangjia Lake West Road, Wuhan 430065, PR China*

[c]*School of Laboratory Medicine, Hubei University of Chinese Medicine, 1 Huangjia Lake West Road, Wuhan 430065, PR China. E-mail: zhanggj@hbtcm.edu.cn; shui10123@aliyun.com; Fax: +86-27-68890259; Tel: +86-27-68890259*

† Electronic supplementary information (ESI) available. See DOI: 10.1039/d0ra10157e

In addition, Zhou *et al.*[19] developed a sensitive electrochemical biosensor-based G-quadruplex DNA-zyme and Au–Pd hybrid nanostructures to detect Pb^{2+}. However, these methods still have some issues, such as, complex operation, high cost, and are time-consuming to use. Therefore, novel methods for the detection of Pb^{2+} are still desirable.

Nowadays, functionalized nanochannel sensors have become one of the representative electrochemical methods, and have been used as a new platform to detect various ions.[20–24] There are two main features in practical applications of functionalized nanochannel sensors: specificity and signal amplification. Firstly, functionalized nanochannel sensors can provide a highly specific surface area, which allows for an increase in the amount of target modification. Secondly, nanochannel sensors can also offer a confined area at the nanoscale for the interactions between functional molecules and analytes,[25,26] which brings kinetic effects for the easy and frequent transport of reactants in the nanochannel. These two main features are associated with applications in highly specific and sensitive sensing.[27] Nowadays, porous anodized aluminum (PAA) membranes have been employed as the representative base material for a nanochannel sensor, which has advantages, including a controllable shape and pore size, and good stability.[28,29] This sensor is not only able to amplify ion current signals, but also reduces the background noise, leading to excellent detection sensitivity. Moreover, the electrical output of a nanochannel that arises from the ion transport inside of it, can be very sensitive to the ionic concentration, thereby suggesting that it has the potential for detecting heavy metal ions.

In recent years, several nanochannel-based sensors for lead ion detection have been proposed. For example, Hsu *et al.*[30] investigated a pH-regulated conical nanochannel device, which was proposed for detecting trace levels of Pb^{2+}. The current–voltage behavior of the nanochannel was successfully examined, however, the selectivity of this sensor needed further improvement. Cheng *et al.*[31] developed a vertically-ordered mesoporous, silica film decorated nanochannel sensor. Although the detection for Pb^{2+} ions in human serum was successful, the preparation process of the sensor was too complex. These studies demonstrate the feasibility and promise of the nanochannel system in the construction of highly-efficient ion sensing devices. However, few studies for detecting Pb^{2+} ions in TCM with PAA-based nanochannels have been reported.

In the work reported here, a peptide-functionalized nanochannel sensor was developed, with the aim of detecting Pb^{2+} in TCM. After the peptide, which is specific to Pb^{2+}, was modified on the surface of the nanochannel, ions except for Pb^{2+} could get through the channel. The peptide can specifically bind the target Pb^{2+} when it appears. Upon binding, the charge on the surface of the nanochannel increases. The conjugated peptide-Pb^{2+} folds, and the effective channel diameter increases. Both the change in charge on the nanochannel surface and the conformational transition lead to concentration-dependent changes in the nanochannel current. This study provides a novel metal ion sensor for TCM quality control by incorporating a Pb^{2+}-binding peptide into the nanochannel. The merits of the assay developed include: (1) high sensitivity and specificity, (2) a strong anti-interference ability in detecting the Pb^{2+} in complex TCM samples, and (3) easy operation without use of expensive instrumentation.

Experiments

Reagents

(3-Aminopropyl) trimethoxysilane (APTES, 98%) and glutaraldehyde solution (25% in H_2O) were purchased from Sigma-Aldrich (St. Louis, MO, USA). The peptide sequences (NH_2-KVSATDADDDVLL-COOH) were synthesized by GL Biochem Ltd. (Shanghai, China) and its isoelectric point is 3.5. The PAAM (60 μm thick, 30 ± 5 nm aperture) were purchased from PuYuan Nanotechnology (Hefei, China). Tris–HCl (pH = 7.5) and potassium chloride (KCl) were purchased from Solarbio (Beijing, China). Arsenic(III), cadmium(II), chromium(III), cobalt(II), iron(III), mercury(II), nickel(II), and zinc(II) standards for AAS were purchased from Macklin (Shanghai, China). Copper(II) sulfate, lead(II) nitrate and manganese(II) chloride were purchased from Sinopharm Chemical Reagent Beijing Co., Ltd. (SCRC, China). All solutions were prepared in Milli-Q water (18.2 MΩ).

Instruments

The nanoporous alumina film was clamped in the middle of two testing cells, which were filled with 5 mM Tris–HCl and 100 mM KCl (pH 7.5). The electrical signal was measured using a Keithley 6487 picoammeter with Ag/AgCl electrodes in two electrochemical cells. The scanning voltage was set from −1 to 1 V. The scanning electron microscopy (SEM) images were obtained using a GeminiSEM system (Zeiss, Germany). The contact angle images were taken using a contact angle measurement system, OCA 20 (Dataphysics Instruments, Germany). The conformational switching of the peptide was determined using circular dichroism (CD) spectra (Applied Photophysics Ltd., UK). Wavelength scans were performed between 185 and 250 nm, and a 10 mm quartz cell was used. The Tris–HCl buffer solutions (10 mM, pH 7.5) with 100 μM of peptide and 100 μM of Pb^{2+} were incubated at 25 °C for 1 h before measurements were made.

Chemical modification of nanochannels

The thickness of the PAAM was about 60 μm and the pore size was about 30 ± 5 nm. The PAAMs were firstly washed with ethanol and ultra-pure water for 5 min using an ultrasonic cleaner. Then, they were soaked in 5% HCl solution for 90 s and the rinsed with ultra-pure water and dried under nitrogen. Secondly, the prepared PAAMs were dipped in ethanol solution containing 5% APTES for 12 h. Then, the PAAMs were washed with ethanol and placed on a heating plate at 140 °C for 1 h. Then, the PAAMs were immersed in a 25% aqueous glutaraldehyde solution overnight. Finally, the membranes were washed with ultra-pure water and dried under nitrogen.

Peptide immobilization and optimization

The peptide was attached to chemically modified PAAM in the test buffer (5 mM Tris–HCl, 100 mM KCl, pH 7.5) by a condensation reaction between glutaraldehyde and the carboxyl group from the peptide. Afterwards, the immobilized PAAM membrane was gently washed with deionized water and stored in the test buffer. The concentration of the immobilized peptide was optimized from 1 to 250 μM, and the modification time was 0.5 h to 5 h. Their action

temperature was optimized from 10 to 40 °C. After optimization of the experimental conditions, the membranes were immersed into the solution containing 100 μM peptide at 25 °C for 3 h. Afterwards, a 10 mg mL^{-1} BSA solution was used to block the unreacted active sites for 1 h to reduce non-specific adsorption, and then the membranes were washed with ultrapure water.

Preparation of herbal medicines prior to lead ion analysis

Herbal medicine samples including Astragali Radix (Huang Qi), Glycyrrhizae Radix et Rhizoma (Gan Cao), American ginseng (Xi Yang Shen) and Lonicerae japonicae flos (Jin Yinhua) were obtained from the Hubei Tianjin Chinese Herbal Pieces Company (Wuhan, China). After the TCM samples were completely ground, 0.5 g samples of the ground powder were dissolved in 10 mL of test buffer, filtered through a 0.45 μm membrane, and then analyzed using the proposed method. At the same time, the extracts, pretreated as previously mentioned, were analyzed by AAS with a graphite tube atomizer (Agilent 200, Agilent Technology Co., Ltd., USA), the gold standard Pb^{2+} ion detection method, was applied to detect Pb^{2+} in the four herbal medicines for a comparison of the method.

Results and discussion

The principle of a peptide-modified nanochannel for Pb^{2+} detection

The working mechanism of the peptide-modified nanochannel biosensor for the detection of Pb^{2+} is shown in Fig. 1. After pre-modification, the Pb^{2+}-specific peptides were immobilized in the nanochannel, where the Pb^{2+} was selectively captured by this specific peptide. It has been reported previously that aspartic acid was used as a recognition ligand for the detection of Pb^{2+} and that it showed a strong interaction with the lead ions.[32] In this work, the sequence of the peptide that was chosen resulted in a specific response of the Pb^{2+} due to its aspartic acids and it had been used previously in the design of a peptide-based electrochemical sensor for the detection of lead ions.[33] Prior to the chemical modification, the nanochannels were treated with sulfuric acid. The hydroxyl groups (–OH) were then exposed on the unmodified nanochannels' surfaces, which were positively charged.[34] After the nanochannel was modified by negatively charged peptides, the charge density of the nanochannel surface decreased. When the Pb^{2+} were bound to the peptide, the charge density of the nanochannel surface dramatically increased due to the contribution of the positively-charged Pb^{2+}. Moreover, the Pb^{2+}-specific peptide blocks the nanochannel, and after adding Pb^{2+}, the blocking effect could be verified as "open" and the ion current increased significantly. As a result of the change in charge density on the nanochannel surface and the conformational transition of the Pb^{2+}-specific peptide, the behavior of the current–voltage (*I–V*) curves changed significantly, resulting in a significant increase of the current.

Optimization of nanochannel modification

To achieve the best optimal modification efficiency, some factors, including temperature, reaction time, and peptide concentration were adjusted to optimize the experimental

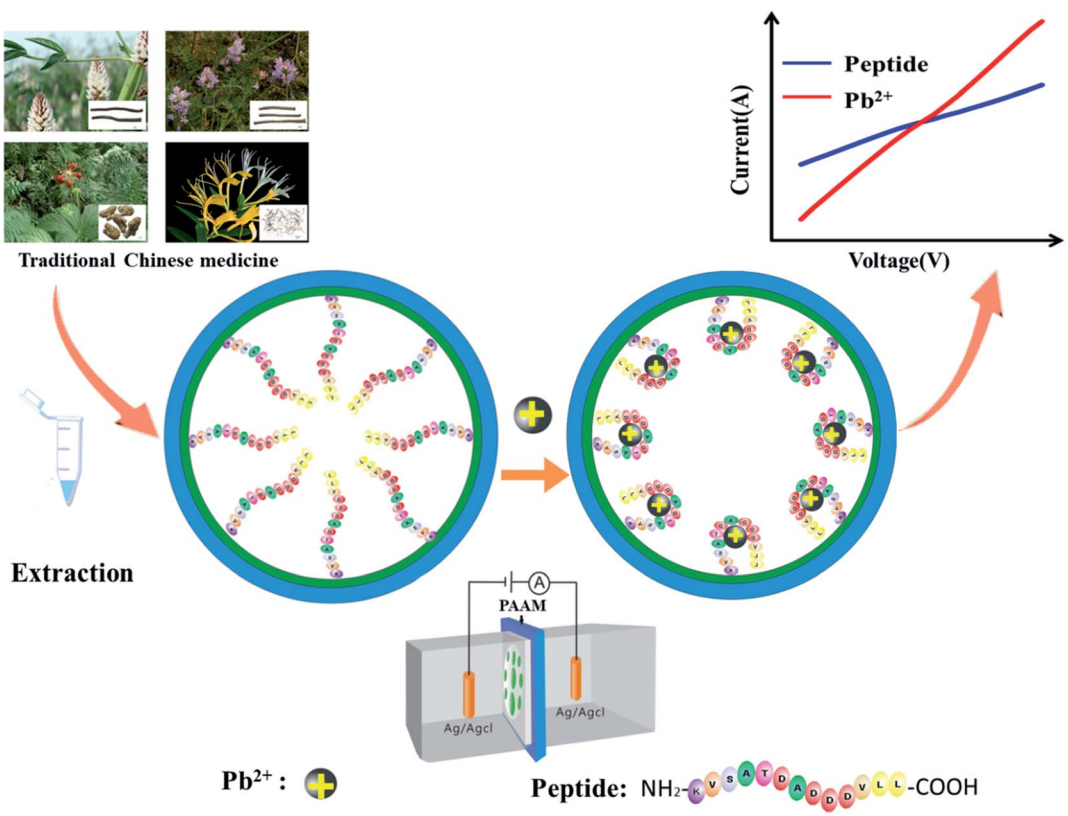

Fig. 1 A schematic diagram of the peptide-modified nanochannel sensor for analysis of Pb^{2+} in TCM.

parameters for peptide immobilization. At a voltage of −1 V, $(I - I_0)/I_0$ was defined as the absolute value of the current change ratio, where I_0 and I were the current values measured at −1 V before and after modification with the peptide, respectively. According to what was observed in the experiments the temperature was the most significant factor affecting the modification effect. As shown in Fig. S4A (ESI†), the optimal temperature was 25 °C. The stability of the imine bond varied with the environment, and a long term treatment may cause the bond to break. This can also be observed in Fig. S4B and C (ESI†). The optimal reaction time and peptide concentration were 3 h and 100 μM, respectively. When the modification time was too long, the blocking effect was less apparent.

Modification and characterization of the nanochannels

In this work, 30 ± 5 nm PAAM nanochannels were selected to be modified with the peptide. Initially, alumina nanochannels were chemically modified with peptides by a three-step process that is shown in Fig. 2A. The current–voltage (*I*–*V*) as a current value measurement was extensively applied to verify the

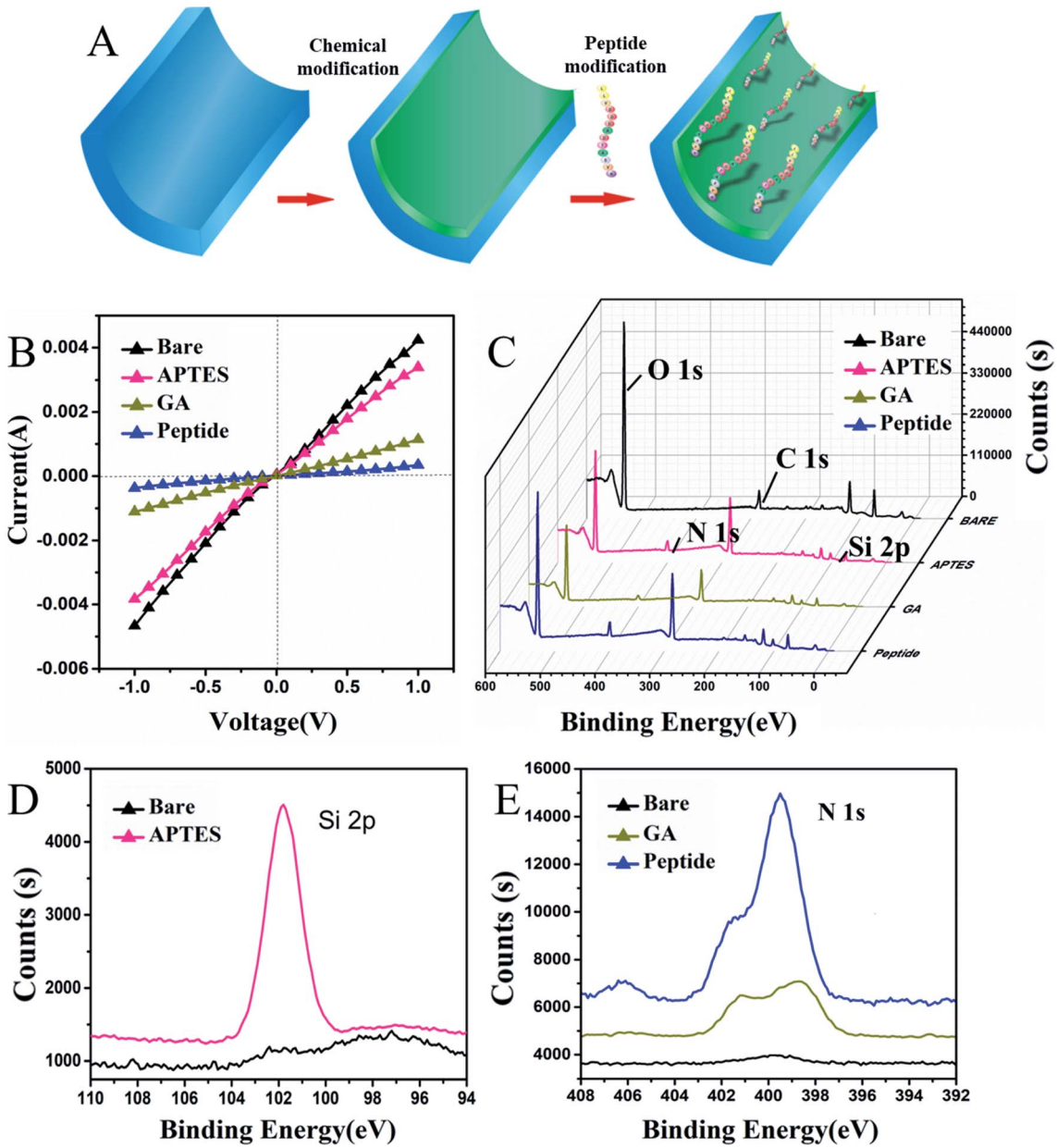

Fig. 2 (A) The modified process. (B) The ion current of the transmembrane before APTES modification (black curve), after APTES modification (pink curve), after GA treatment (brown curve) and after peptide modification (blue) from −1 V to 1 V. (C) The XPS spectra of the PAA membrane without (black) and with modification by APTES (pink), GA (brown), the peptide (blue). (D) Narrow survey of XPS analysis of the silicon of bare and APTES modified PAAM surface. (E) Narrow survey of XPS analysis on nitrogen element of bare, GA and peptide modified PAAM surface, respectively. The peptide concentration was 100 μM, and the current–voltage detection was carried out in buffer (5 mM Tris–HCl, 5 mM KCl, pH 7.5).

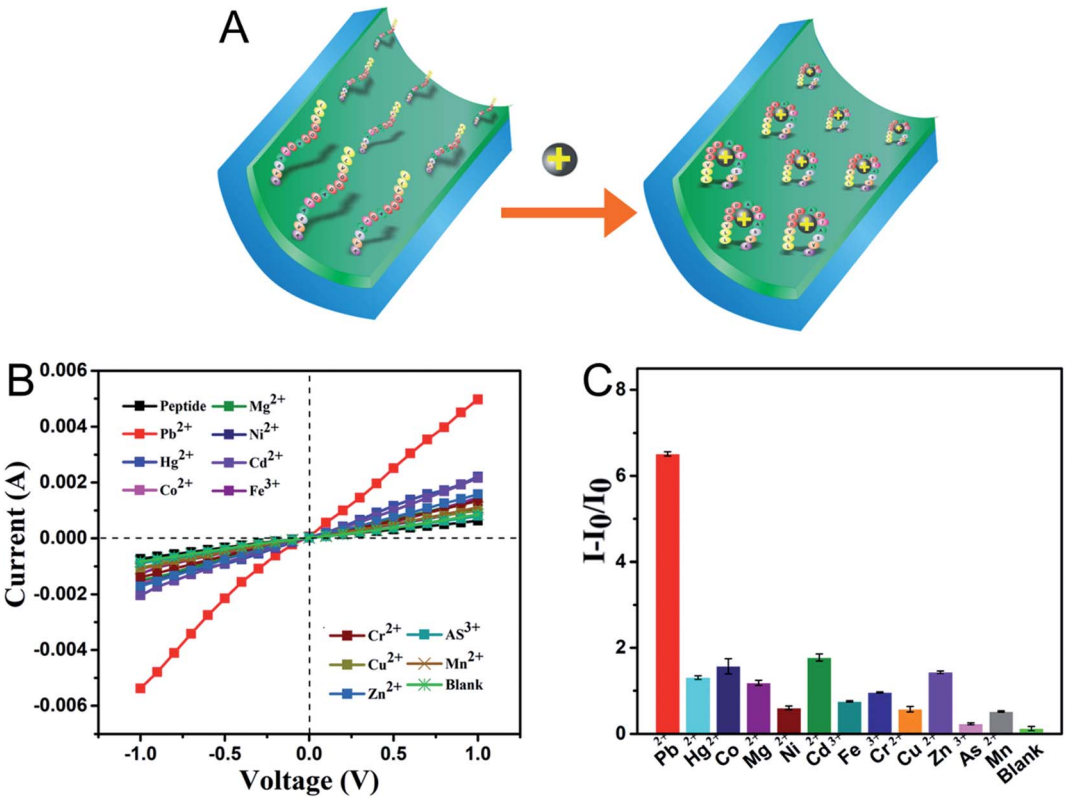

Fig. 3 (A) Binding Pb^{2+} process, (B) and (C) the sensor's responses to 11 different metal ions and Pb^{2+}, the blank contains no metal ions, and the concentration of each metal ion was 100 μM. The concentrations of the peptide and the ions are 50 and 100 μM, respectively.

properties of the modified nanochannels. In the first step shown in Fig. 2B, it is seen that the successful APTES modification resulted in a slight decrease in the current change, which was caused by the change of wettability on its surface.[23] As can also be seen from the contact angle images showed in Fig. S1B (ESI†), the contact angle after the APTES modification increased from 26.6° ± 0.6° to 45.7° ± 1.3°, which proved that the hydrophobicity of the nanochannel surface was increased after APTES modification. After the covalent interaction of glutaraldehyde with APTES, the current decreased significantly because the positive charge on the surface of the nanochannel was reduced when the uncharged glutaraldehyde was successfully applied. These *I–V* curve results were consistent with those presented in previous studies.[35–37] Additionally, the contact angle shown in Fig. S1C (ESI†) further increased because the hydroxyl groups on the surface of the nanochannels were converted to aldehyde groups, thereby proving that the glutaraldehyde on the nanochannel had been modified. After modification with the peptide, the modified peptide blocked the nanochannel, which decreased the current due to the conformational transition of the peptide. In addition, the peptides with amino acids, which had a strong hydrophilicity, also decreased the contact angle as shown in Fig. S1D (ESI†), indicating that the peptide was modified successfully. Thereafter, the unreacted active sites on the channel surface were blocked with 10 mg mL^{-1} BSA, and no significant change in current was observed because of the reduced number of unreacted active sites.

To further demonstrate that the surface modification of the nanochannel had occurred, X-ray photo electron spectroscopy (XPS) and SEM characterization of the peptide attachment was performed. It is shown in Fig. 2C and D, that the bare PAAM does not show the Si 2p peak (black curve), whereas a distinct peak of Si 2p appears (pink curve) after the ion nanochannel was treated with APTES, indicating the successful immobilization of APTES. There are plenty of Al–OH groups on the PAAM, and after coupling with APTES and GA, the Al–OH groups transformed into reactive aldehyde groups that can be used for covalent binding of the peptide. As shown in Fig. 2E, unmodified PAAM (black line) has no significant N 1s peaks. However, after the APTES modification occurred, a clear peak of N 1s was observed on the PAAM membrane (brown line), which also proved that successful immobilization of APTES had happened. Then, after further modification with the peptide (blue line), peaks corresponding to N 1s significantly increased compared with those in the APTES and GA modification step because of the presence of nitrogen in the peptide. Moreover, the morphology of the prepared PAAMs and peptide-modified PAAMs were characterized using SEM, as shown in Fig. S2 (ESI†). After modification with the peptide, it can be seen in Fig. S2B and D (ESI†), that the surface of the PAAM was covered with the peptide, which decreased the internal diameter of the nanochannels from 33 nm to 27 nm due to the modification of the peptide compared with the unmodified PAAMs shown in Fig. S2A and C (ESI†). Overall, the XPS and

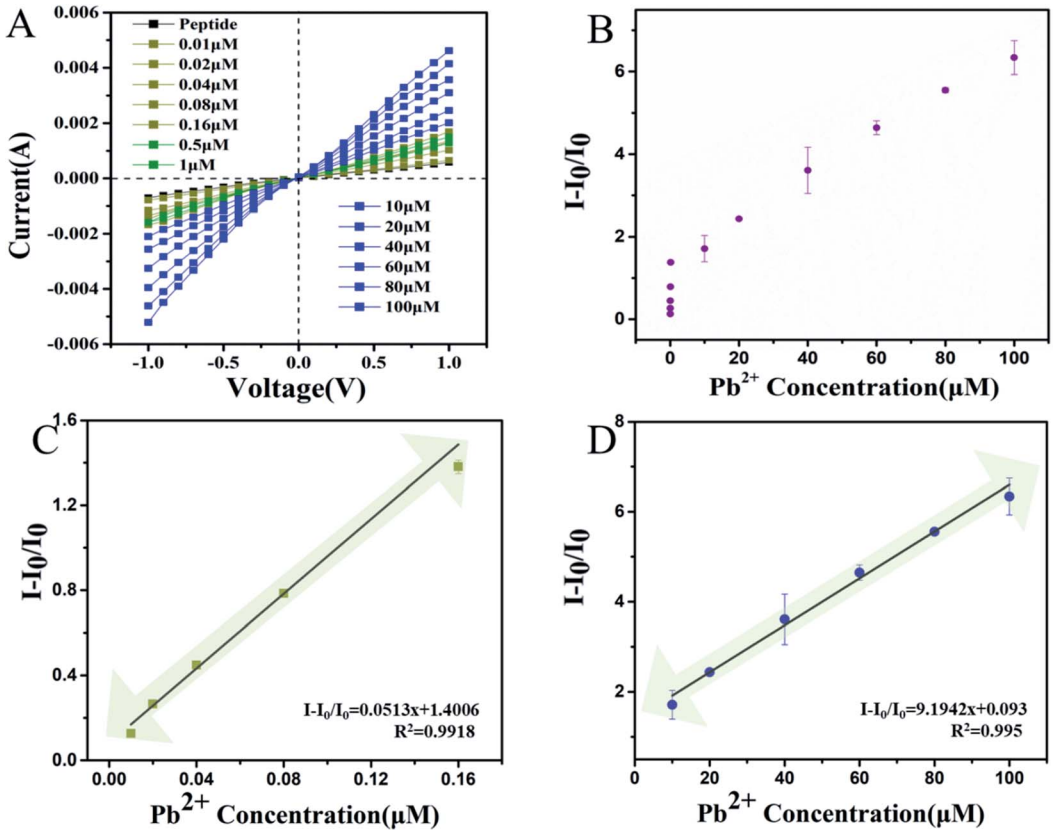

Fig. 4 (A) The I–V curves of the nanochannel biosensor bound with Pb^{2+}, measured at a series of concentrations (0.01 μM to 100 μM). (B) The linear relationship between the $I - I_0/I_0$ value and the concentration of Pb^{2+} (0.01 μM to 0.16 μM and 10 μM to 100 μM). (C) The linear relationship between the $I - I_0/I_0$ value of the Pb^{2+} concentration from 0.01 μM to 0.16 μM. (D) The linear relationship between the $I - I_0/I_0$ value of the Pb^{2+} concentration from 10 μM to 100 μM.

SEM characterization results indicated that the peptide-modification on the nanochannel surface was successful.

Selectivity of the nanochannel sensor

The selectivity of the sensor system to the peptide-modified nanochannel sensor was tested by applying various ions, including As^{3+}, Cd^{2+}, Co^{2+}, Cr^{3+}, Cu^{2+}, Fe^{3+}, Hg^{2+}, Mg^{2+}, Mn^{2+}, Ni^{2+}, and Zn^{2+}. The prepared sensor was immersed in a solution containing 100 μM of interfering metal ions, and for the blank, test buffer without metal ions was used. As shown in Fig. 3B and C, the current–voltage curves showed that under the same experimental conditions, the current response of the Pb^{2+} solution was the highest and the control only responded very slightly. After adding Pb^{2+}, the I–V results presented in Fig. 3A show that the current increased significantly, which was due to the change in the charges on the surface and the peptide conformation in the nanochannel. The sensor responded slightly to other ions, such as Cd^{2+}, Co^{2+}, and Mg^{2+}, and the signal change was significantly less when compared to that of Pb^{2+}. The corresponding ion current change ratios ($I - I_0/I_0$) of the modified nanochannel in the presence of test ions are shown in Fig. 3C. The I_0 and I are the current values measured before and after adding the metal ions, respectively. It was obvious that the relative ion current change ratio for Pb^{2+} was much bigger than that of other ions. Thus, the data given above indicate that the nanochannel sensor can detect Pb^{2+} among other metal ions, exhibiting remarkable selectivity.

Table 1 Determination of Pb^{2+} in traditional Chinese medicine samples ($n = 3$)

		Determined (AAS)		Determined (PAAM)		
Sample	Origin (No.)	nM	mg kg^{-1}	nM	mg kg^{-1}	Recovery (%)
Astragali radix	Neimeng (201905030TJ)	16.9 ± 1.4	0.30 ± 0.0125	19.26 ± 0.9	0.31 ± 0.0167	87.7
Glycyrrhizae radix et rhizoma	Neimeng (190410TQT)	30.2 ± 1.6	0.2 ± 0.0972	28.9 ± 1.2	0.17 ± 0.0141	104.5
American ginseng	Hebei (201812004TJ)	37.7 ± 6.8	0.33 ± 0.002	32.27 ± 0.24	0.39 ± 0.0707	116.8
Lonicerae japonicae flos	Hebei (201906001TJ)	126.9 ± 3.7	1.28 ± 0.009	123.9 ± 9.3	1.31 ± 0.0357	102.4

Verification of the successful capture of Pb^{2+}

To further verify the successful capture of Pb^{2+} (Fig. 3A), XPS and CD experiments were carried out. The XPS results in Fig. S3B (ESI†) show that after Pb^{2+} was added, the Pb 4f (140 eV) peak appeared. To clearly evaluate the reaction between the peptide and Pb^{2+}, CD experiments were carried out. The CD is a useful spectroscopic technique applied for studying the peptide structure in solution, which can show the conformational switching of the peptide, including α-helixes, β-pleated sheets, and other changes.[38] As shown in Fig. S3A (ESI†), the CD experiments in the peptide solution showed a positive peak near 190 nm. After the addition of Pb^{2+}, the peak became too negative. Moreover, the negative peak near 200 nm decreased after adding Pb^{2+}.These results indicated that the α-helicity of the peptide decreased, which induced the diameter to decrease after adding Pb^{2+} ions.[39] The decrease in hindrance caused an increase in the current, which further showed the mechanism of this peptide-based nanochannel system. The previously mentioned results demonstrated that the Pb^{2+} was successfully captured.

Sensitivity

Based on the optimal experimental conditions, the lowest Pb^{2+} concentration was determined. The results of this are shown in Fig. 4A and B. The current increased after the Pb^{2+} binding within a certain range from −0.789 μA to −5.21 μA at a voltage of −1 V. In Fig. 4C and D, it is shown that the $I - I_0/I_0$ was linearly related to the concentration of Pb^{2+} from 0.01 to 0.16 μM. The linear relationship between the Pb^{2+} concentration and $I - I_0/I_0$ can be described by the expression: $I - I_0/I_0 = 9.1942x + 0.093$ and $I - I_0/I_0 = 0.0513x + 1.4006$ with correlation coefficients of $R^2 = 0.995$ and $R^2 = 0.9918$, respectively. This strategy yielded a low detection limit of 0.005 μM. As shown in Table S1 (ESI†), the papers published on the detection of Pb^{2+} are summarized. These include carbon nanotubes, graphene quantum dots, fluorescence probes and other methods have also been gradually developed. Compared with the other methods shown in Table S1 (ESI†), this method has obvious advantages such as lower limits of detection at 5 nM and better sensitivity. Unlike the other methods, which all have their own limits for detecting complex samples, this method has advantages for the detection of in TCM samples which has potential applications in toxic heavy metals research.

Pb^{2+} analysis in TCM

To evaluate whether this peptide-modified nanochannel sensor can be applied to the quantification of Pb^{2+} in TCM, four representative practical samples from TCM: Astragali radix, Glycyrrhizae Radix et Rhizoma, American ginseng, and Lonicerae japonicae Flos were employed. Detection of the Pb^{2+} content in these samples was carried out as mentioned previously, and the results were compared with the results of the gold standard method (AAS). As shown in Table 1, the results of this sensor were consistent with those of AAS for the determination of Pb^{2+} in TCM. The data show that compared with the AAS method, the recovery of the peptide-modified nanochannel sensor was between 87.7% and 116.8%. Thus, these experimental results proved that this new sensor is a good choice for the accurate detection of Pb^{2+} in TCM samples.

Conclusion

In conclusion, a peptide-modified nanochannel sensor, was designed which has high sensitivity and selectivity for the detection of Pb^{2+}. By changing the ionic current signal, the microstructural change in this peptide-based nanochannel sensor caused by Pb^{2+} could be easily and sensitively monitored. In addition, this system exhibited an ultra-trace selective recognition ability to Pb^{2+} at a very low concentration (about 5 nM) and did not interact with other heavy metal ions including: As^{2+}, Cd^{3+}, Co^{2+}, Cr^{2+}, Cu^{2+}, Fe^{3+}, Hg^{2+}, Mg^{2+}, Mn^{2+}, Ni^{2+}, and Zn^{2+}. Moreover, the detection was selective enough to be applied in complex TCM samples, which provides a potentially convenient assay for applications in environmental and biological samples. With further optimization, this sensor can potentially be applied in commercially portable devices for the detection of various metal ions in TCM without the use of expensive instruments and complex preparation procedures.

Funding information

This work was supported by the National Natural Science Foundation of China (Grant No. 21974035).

Conflicts of interest

The authors declare that there are no conflicts of interest.

References

1 P. Li, L. P. Yang and Y. W. Gong, *J. Tradit. Chin. Med.*, 2009, **29**, 153–157, DOI: 10.1016/S0254-6272(09)60054-6.
2 J. Qiu, *Nature*, 2007, **446**, 590–591, DOI: 10.1038/446590a.
3 X. Chen, H. Zhou, Y. B. Liu, J. F. Wang, H. Li, C. Y. Ung, L. Y. Han, Z. W. Cao and Y. Z. Chen, *Br. J. Pharmacol.*, 2006, **149**, 1092–1103, DOI: 10.1038/sj.bjp.0706945.
4 H. F. Ji, X. J. Li and H. Y. Zhang, *EMBO Rep.*, 2009, **10**, 194–200, DOI: 10.1038/embor.2009.12.
5 G. Wang, B. Mao, Z. Y. Xiong, T. Fan, X. D. Chen, L. Wang, G. J. Liu, J. Liu, J. Guo, J. Chang, T. X. Wu and T. Q. Li, *Clin. Therapeut.*, 2007, **29**, 1456–1467, DOI: 10.1016/j.clinthera.2007.07.023.
6 F. Tang, Q. Zhang, Z. Nie, S. Yao and B. Chen, *Trac. Trends Anal. Chem.*, 2009, **28**, 1253–1262, DOI: 10.1016/j.trac.2009.09.004.
7 K. Chan, *Chemosphere*, 2003, **52**, 1361–1371, DOI: 10.1016/S0045-6535(03)00471-5.
8 D. Melucci, M. Locatelli and C. Locatelli, *Food Chem. Toxicol.*, 2013, **62**, 901–907, DOI: 10.1016/j.fct.2013.10.029.
9 X. P. Lu, X. A. Yang, L. Liu, H. H. Hu and W. B. Zhang, *Talanta*, 2017, **165**, 258–266, DOI: 10.1016/j.talanta.2016.12.070.

10 National Pharmacopoeia Committee, *Pharmacopoeia of People's Republic of China*, People's Medical Publishing House, Beijing, China, 2020, part 4, p. 234.
11 F. Zhou, G. Du, J. Xie, J. Gu, Q. Jia, Y. Fan, H. Yu, Z. Zha, K. Wang, L. Ouyang, L. Shao, C. Feng and G. Fan, *Sci. Total Environ.*, 2020, **701**, 134901, DOI: 10.1016/j.scitotenv.2019.134901.
12 Y. Finkelstein, M. E. Markowitz and J. F. Rosen, *Brain Res. Rev.*, 1998, **27**, 168–176, DOI: 10.1016/S0165-0173(98)00011-3.
13 X. Zheng, X. Huo, Y. Zhang, Q. Wang, Y. Zhang and X. Xu, *Environ. Pollut.*, 2019, **246**, 587–596, DOI: 10.1016/j.envpol.2018.12.055.
14 S. A. Sudjarwo, G. W. Sudjarwo and Koerniasari, *Results Pharma Sci.*, 2017, **12**, 381–390, DOI: 10.4103/1735-5362.213983.
15 N. Alvarez-Ortega, K. Caballero-Gallardo and J. Olivero-Verbel, *Environ. Int.*, 2019, **130**, 104809, DOI: 10.1016/j.envint.2019.05.003.
16 Z. Khoshbin, M. R. Housaindokht, A. Verdian and M. R. Bozorgmehr, *Biosens. Bioelectron.: X*, 2018, **116**, 130–147, DOI: 10.1016/j.bios.2018.05.051.
17 Z. Dahaghin, P. A. Kilmartin and H. Z. Mousavi, *Food Chem.*, 2020, **303**, 125374, DOI: 10.1016/j.foodchem.2019.125374.
18 A. Shah, A. Satti, A. Khan, F. Iftikhar, J. Nisar, C. Fernandez, M. Akhter, A. Almutawah and H. Kraatz, *J. Electrochem. Soc.*, 2019, **166**, B3136–B3142, DOI: 10.1149/2.0271909jes.
19 B. Niu, K. Xiao, X. Huang, Z. Zhang, X. Y. Kong, Z. Wang, L. Wen and L. Jiang, *ACS Appl. Mater. Interfaces*, 2018, **10**, 22632–22639, DOI: 10.1021/acsami.8b05686.
20 Y. Tian, X. Hou, L. Wen, W. Guo, Y. Song, H. Sun, Y. Wang, L. Jiang and D. B. Zhu, *Chem. Commun.*, 2010, **46**, 1682–1684, DOI: 10.1039/B918006K.
21 X. P. Zhao, S. S. Wang, M. Younis and X. H. Xia, *Anal. Chem.*, 2017, **90**, 239–246, DOI: 10.1021/acs.analchem.7b03818.
22 R. Mo, Q. Yuan, X. Yan, T. Su, Y. Feng, L. Lv, C. Zhou, P. Hong, S. Sun and C. Li, *J. Electrochem. Soc.*, 2018, **165**, H750–H755.
23 R. Mo, L. He, X. Yan, T. Su, C. Zhou, Z. Wang, P. Hong, S. Sun and C. Li, *Electrochem. Commun.*, 2018, **95**, 9–13, DOI: 10.1016/j.elecom.2018.08.012.
24 H. Y. Wang, Z. Y. Song, H. S. Zhang and S. P. Chen, *Microchim. Acta*, 2016, **183**, 1003–1010, DOI: 10.1007/s00604-015-1699-x.
25 H. Zhang, Y. Tian and L. Jiang, *Nano Today*, 2016, **11**, 1003–1010, DOI: 10.1016/j.nantod.2015.11.001.
26 J. Shi, J. Hou and Y. Fang, *Microchim. Acta*, 2016, **183**, 925–939, DOI: 10.1007/s00604-015-1503-y.
27 H. Zhang, Y. Tian and L. Jiang, *Nano Today*, 2016, **11**, 61–81, DOI: 10.1016/j.nantod.2015.11.001.
28 K. Xiao, K. Wu, L. Chen, X. Y. Kong, Y. Zhang, L. Wen and L. Jiang, *Angew. Chem.*, 2017, **130**, 151–155, DOI: 10.1002/anie.201708695.
29 M. Amouzadeh Tabrizi, J. Ferré-Borrull and L. F. Marsal, *Microchim. Acta*, 2020, **187**, 230, DOI: 10.1007/s00604-020-4188-9.
30 J. P. Hsu, T. C. Su, C. Y. Lin and S. Tseng, *Electrochim. Acta*, 2018, **294**, 84–92, DOI: 10.1016/j.electacta.2018.10.074.
31 B. Cheng, L. Zhou, L. Lu, J. Liu, X. Dong, F. Xi and P. Chen, *Sens. Actuators, B*, 2017, **259**, 364–371, DOI: 10.1016/j.snb.2017.12.083.
32 S. J. Li, N. Xia, B. Yuan, W. M. Du, Z. F. Sun and B. B. Zhou, *Electrochim. Acta*, 2015, **159**, 600–604, DOI: 10.3109/10799893.2015.1030412.
33 N. Yusof, N. Daud, S. Saat, T. Tee and A. Abdullah, *Int. J. Electrochem. Sci.*, 2012, **7**, 10358–10364.
34 X. Zhang, L. Zhang and J. Li, *Anal. Chim. Acta*, 2019, **1057**, 36–43, DOI: 10.1016/j.aca.2019.01.018.
35 A. de la Escosura-Muñiz and A. Mekoçi, *Chem. Commun.*, 2010, **46**, 9007–9009, DOI: 10.1039/C0CC02683B.
36 T. Liao, X. Li, Q. Tong, K. Zou, H. Zhang, L. Tang, Z. Sun and G.-J. Zhang, *Anal. Chem.*, 2017, **89**, 5511–5518, DOI: 10.1021/acs.analchem.7b00487.
37 C. Wang, D. Jin, Y. Yu, L. Tang, Y. Sun, Z. Sun and G. J. Zhang, *Sens. Actuators, B*, 2020, **314**, 128056, DOI: 10.1016/j.snb.2020.128056.
38 N. Greenfield, *Trac. Trends Anal. Chem.*, 1999, **18**, 236–244, DOI: 10.1016/S0165-9936(98)00112-5.
39 R. Chenthattil and J. G. Manjunatha, *J. Anal. Sci. Technol.*, 2020, **11**, 3, DOI: 10.1186/s40543-019-0194-0.